inorganics

MDPI

Article

The Melt of Sodium Nitrate as a Medium for the Synthesis of Fluorides

Pavel Fedorov [1,2,*], Mariya Mayakova [1], Alexander Alexandrov [2], Valery Voronov [1], Sergey Kuznetsov [1], Alexander Baranchikov [3] and Vladimir Ivanov [3]

[1] Prokhorov General Physics Institute, Russian Academy of Sciences, 38 Vavilov Street, Moscow 119991, Russia; mn.mayakova@gmail.com (M.M.); voronov@lst.gpi.ru (V.V.); kouznetzovsv@gmail.com (S.K.)
[2] Institute of Fine Chemical Technology, Moscow Technology University, 86 Vernadsky Prospect, Moscow 119571, Russia; alexandrov1996@yandex.ru
[3] Kurnakov Institute of General and Inorganic Chemistry, Russian Academy of Sciences, 31 Leninskii Prospect, Moscow 119991, Russia; a.barantchikov@gmail.com (A.B.); van@igic.ras.ru (V.I.)
* Correspondence: ppfedorov@yandex.ru; Tel.: +7-499-503-8292

Received: 5 March 2018; Accepted: 28 March 2018; Published: 29 March 2018

check for updates

Abstract: The preparation of $NaLnF_4$ complexes, LnF_3 (Ln = La, Ce, Y) rare earth binary fluorides, CaF_2 and SrF_2 alkali earth fluorides, as well as mixtures of these compounds from their nitrates dissolved in molten $NaNO_3$ has been studied in order to select the ideal solvent for fluoride synthesis by spontaneous crystallization from flux. Sodium fluoride (NaF) was used as a fluorinating agent. The results of our experiments have confirmed that $NaNO_3$ melt is one of the most promising media for precipitating said inorganic fluoride materials within a broad temperature range (300–500 °C). Also, in contrast with precipitation/co-precipitation from aqueous solutions, our syntheses have resulted in obtaining equilibrium phases only.

Keywords: fluorides; sodium nitrates; flux; fluorite; inorganic synthesis

1. Introduction

Inorganic fluorides can be prepared using a broad variety of techniques [1–6]. However, using these methods in practice is always accompanied by some experimental obstacles. The most important problem for the fluoride syntheses is the reaction of said fluorides with water, i.e., hydrolysis, which leads to an accumulation of hydroxyl and/or oxygen impurities in the obtained materials [7–9]. Atmospheric water vapor, water from aqueous solutions and/or water adsorbed on the solid particle surfaces can participate in hydrolyzing fluorides. The rate of hydrolytic chemical transformation increases significantly when temperature goes up and hydrolysis at an elevated temperature has been called pyrohydrolysis. In order to suppress hydrolysis, an excess of fluorinating agent has been widely implemented to create a proper fluorinating atmosphere [10,11]. Direct oxidation by molecular oxygen in the course of fluorination is usually unfavorable from a thermodynamics point of view and, thus, as a result, it usually does not create additional problems for fluoride syntheses.

Undesirable batch reactions with crucible materials are important factors in solid phase fluorination and syntheses in molten media [2,12,13]. Typically, the use of ceramic crucibles is not possible due to their corrosion accompanied by the formation of highly volatile fluoride by-products, such as SiF_4 and/or AlF_3. On the other hand, metal (Mo, Ni, Cu, steel, etc.) or carbon crucibles can efficiently reduce fluorides, lowering the oxidation state of the fluoride-forming metal (europium, ytterbium) [14,15] or even completely reducing the latter to the free element (bismuth) [16]. Gold [17] and copper [18] seem to be convenient materials for fluoride preparation, but, nevertheless, one has to consider that hermetically sealed reactors are preferred in comparison to unsealed crucibles [17,19], for even platinum can become a reducing agent in the opened systems [20,21]. Teflon and/or other organofluorine polymers also can be used for the synthesis of fluorides with lower melting points and higher reaction activities [22,23].

The sintering time that is necessary for reaching the solid-phase equilibrium increases exponentially with a temperature decrease, and this factor becomes an overwhelming obstacle for the low-temperature phase synthesis [13,24].

Non-equilibrium specimens with unique functional properties (e.g., enhanced ionic conductivity) can be obtained by mechanochemical techniques. The use of such methods leads to product contamination with milling materials, such as ZrO_2 or WC. However, a detailed study of possible oxygen contamination of the mechanochemical synthesis products has yet to be carried out [6,25].

Various functional fluoride materials with highly developed surfaces have been synthesized by thermal decomposition of the corresponding trifluoroacetates [6,26,27]. This is a very attractive synthetic method, but it leads to the product's contamination with elemental carbon.

In contrast with the solid-phase synthesis, the use of solvents leads to a very significant rate acceleration. Water is the simplest solvent, and most fluorides, having low solubility in it, can be easily precipitated from aqueous solutions [3,4,28]. Such precipitation is very inexpensive. It requires very simple experimental arrangements and, very frequently, leads to the formation of nanofluorides [3,4,28]. Precipitation at room temperature minimizes hydrolysis by-products, but a well-developed surface of fluoride nanoparticle makes said hydrolysis easier. For example, hydrolytic oxygen contamination has been observed for bismuth fluoride precipitation [29].

We have performed systematic studies of phase formation in the fluoride systems using co-precipitation from aqueous nitrate and/or citrate solutions by various fluorinating agents (e.g., hydrofluoric acid, sodium fluoride, ammonium fluoride, etc.) [3,4,29–39]. Our results are valuable from both practical (luminophores, laser ceramics precursors, solid electrolytes) and theoretical (studying non-classic crystallization mechanism via oriented attachment crystal growth [40]; making novel non-equilibrium phases of variable compositions [30]) points of view. Our results have revealed a broad variety of the synthesized material properties compared to the existing data for the known phase diagrams obtained under equilibrium conditions [34]: low solubilities of the precipitated fluorides hindered achieving the chemical equilibrium.

It is worth noting that nanofluorides, obtained by co-precipitation, are hydrated. Highly active nanopowder surfaces causes multilayered water adsorption [41]. This hydration leads to the formation of quite unusual chemical compounds, such as $(H_3O)Ln_3F_{10}$ (Ln = rare-earth elements) [30,42], and causes luminescence quenching by OH^- groups and/or water molecules in freshly prepared nanopowders. It is not easy to remove water that has been adsorbed on nanoparticle surfaces but their pyrohydrolysis under thermal treatment can be prevented by forming compounds with fluorinating agents, such as $BaF_2 \cdot HF$ [37] or ammonium fluoride solid solutions in strontium fluoride, $Sr_{1-x-y}Ln_x(NH_4)_yF_{2+x-y}$ [34,38,39].

By definition, hydrothermal syntheses occur at elevated temperatures. This leads to a solubility increase and a surface energy decrease (particle faceting) for the synthesized nanofluorides, and equilibrium conditions can be reached. We successfully used the aforementioned hydrothermal techniques to prepare potassium—rare earth fluoride compound series [43–45] and, thus, refined phase equilibria data (including the ones for the lower temperatures) for the $KF–RF_3$ systems [46]. However, temperature increase is accompanied with hydrolysis acceleration, and the content of the contaminating oxygen admixtures also increases in the $K_2RF_5 < KRF_4 < KR_2F_7 < KR_3F_{10}$ series due to the isomorphous substitution of fluorine ions by OH^- fragments with preservation of the phase homogeneity.

Shifting from water to organic solvents (i.e., shifting from hydrothermal to solvothermal methods) helps overcome the hydrolysis problem [3,4,47–49].

Molten salt synthesis (MSS) represents an additional group of synthetic techniques. These techniques include phase formation and crystallization from molten solutions (flux) and it requires the used solvents to have lower melting temperatures, be chemically inert (i.e., solvents shall not form compounds and/or solid solutions with the target compounds or phases), have sufficient solubility for the starting materials, be able to separate solvent from the products, and be non-volatile and display low toxicity [50]. Of course, there is no such thing as an ideal solvent, but one still can try to find the best fitting materials for the aforementioned MSS technology. Sodium fluoride can be considered as one of the most promising MSS materials due to its sufficient water solubility and relatively low melting point (994 °C). However, it easily forms numerous phases with the other fluorides, like in the NaF–BaF_2–GdF_3 system [51]. Other fluoride flux materials for MSS methods include the following examples: Garton and Wanklyn grew K_2NaGaF_6 and Rb_2KGaF_6 single crystals using PbF_2 solvent [52], Hoppe utilized toxic thallium fluoride as a flux [53], and other authors [54] implemented the highly reactive NH_4HF_2 as a flux and fluorinating agent for $KMgF_3$ preparation [54].

$PbCl_2$ can be used as a chloride flux, but it has low water solubility. Courbion et al. synthesized $KGaF_4$ from 3KCl:$ZnCl_2$ molten solution [55]. Fedorov et al. [56,57] prepared CaF_2 and SrF_2 utilizing water soluble calcium and strontium chlorides as fluxes, respectively.

Oxide glasses can be considered as some kind of fluxes, too, as nanofluorides can be obtained from oxyfluoride glass ceramics by a dissolution of the silicate matrix in hydrofluoric acid [58]. However, the aforementioned oxyfluoride glass ceramics are not the only ones representative of exotic type fluxes. Thus, an orthorhombic single CaF_2 crystal polymorph has been grown under high pressure from molten $Ca(OH)_2$ flux [59].

All of the above-listed reasons illustrate the need to search for novel solvents and, as a result, we have explored those opportunities and suggested nitrate melts as such alternative fluxes. Namely, we present below our results for the use of $NaNO_3$ melt for fluoride syntheses.

The earliest reports about fluoride preparations in sodium and potassium nitrate melts, perhaps, were made by Batsanova et al. in 1971 [60,61] but later nitrate melts were implemented again for obtaining up-conversion luminophores [62–66], including the synthesis of doped $LiYF_4$ in molten $NaNO_3$–KNO_3 mixture [62] as well as the preparation of up-conversion luminophores based on $NaYF_4$ [63], $LiYF_4$ [64], $NaBiF_4$ [65], "$BaCeF_5$" [66] phases in ammonium nitrate.

2. Results

In the present paper, we have studied the preparation of well-known LnF_3 (Ln = La, Ce, Y) rare earth and CaF_2, SrF_2 alkali earth fluorides as well as their mixtures and $NaLnF_4$ complexes from solutions of corresponding metal nitrates in molten $NaNO_3$ by spontaneous crystallization (precipitation) in melt solutions. Despite the fact that actual chemical composition of the aforementioned $NaLnF_4$ phases is $Na_{3x}Ln_{2-x}F_6$ (gagarinite-type structure, derived from UCl_3-type; $x \sim 0.5$) [2,32,46], we will name such solid solution compounds formed in the NaF–LnF_3 system as $NaLnF_4$ in agreement with modern literature naming conventions.

We have used sodium fluoride (NaF) as the fluorinating agent in the studied systems; the corresponding chemical transformations can be described by the following equations:

$$Ln(NO_3)_3 + 3NaF \rightarrow LnF_3\downarrow + 3NaNO_3, \qquad (1)$$

$$Ln(NO_3)_3 + 4NaF \rightarrow NaLnF_4\downarrow + 3NaNO_3, \qquad (2)$$

$$M(NO_3)_2 + 2NaF \rightarrow MF_2\downarrow + 2NaNO_3. \qquad (3)$$

Results of our work are presented in Table 1 and Figures 1–10.

2.1. The NaF–YF_3 System

X-ray diffraction patterns of $NaYF_4$ powders, obtained by precipitation from the $NaNO_3$ melt, before (**a**) and after (**b**) washing with water are presented in Figure 1. The most intensive peaks in sample (**a**) X-ray diffraction pattern correspond to $NaNO_3$ phase ($R-3c$ space symmetry group (SSG);

PCPDFWIN # 85-1466). After washing with water, sample (**b**) contained only one phase, $NaYF_4$ or β-$Na(Y_{1.5}Na_{0.5})F_6$ (*P*63/*m* SSG; PCPDFWIN # 16-0334).

Table 1. Conditions and results of fluoride synthesis experiments.

Sample Number *	Ratios of Starting Materials, mol %(M,Ln)$(NO_3)_x$:NaF:$NaNO_3$	Temp. (°C)	Phase Composition	Space Symmetry Group	Crystal Lattice Parameters, Å
1	11:30:59	320	$NaYF_4 + YF_3$	$P6_3/m$ $Pnma$	$a_1 = 5.982(1)$ $c_1 = 3.525(1)$ $a_2 = 6.388(1)$ $b = 6.846(1)$ $c_2 = 4.244(1)$
2	9:39:52	320	$NaYF_4 + YF_3$	$P6_3/m$	$a = 5.982(1)$ $c = 3.525(1)$
3	7:52:41	320	$NaYF_4$	$P6_3/m$	$a = 5.984(1)$ $c = 3.525(1)$
4	7:52:41	435	$NaYF_4$	$P6_3/m$	$a = 5.974(2)$ $c = 3.529(1)$
5	3:6:91	400	LaF_3	$P-3c1$	$a_1 = 7.1815(3)$ $c_1 = 7.3365(2)$
6	90:4:5	330	LaF_3	$P-3c1$	$a = 7.1841(1)$ $c = 7.3522(1)$
7	4:53:43	400	$CeF_3 + NaCeF_4$	$P-3c1$ $P321$	$a_1 = 7.0901(1)$ $c_1 = 7.2481(1)$ $a_2 = 6.1367(2)$ $c_1 = 3.7377(2)$
8	11:67:22	300	CaF_2	$Fm-3m$	$a = 5.4654(1)$
9	6:35:59	300	CaF_2	$Fm-3m$	$a = 5.4655(1)$
10	9:55:36	400	CaF_2	$Fm-3m$	$a = 5.4648(1)$
11	14:29:57	400	CaF_2	$Fm-3m$	$a = 5.4648(1)$
12	11:67:22	300	SrF_2	$Fm-3m$	$a = 5.8010(1)$
13	6:35:59	300	SrF_2	$Fm-3m$	$a = 5.8001(1)$
14	9:55:36	400	SrF_2	$Fm-3m$	$a = 5.8001(1)$
15	20:40:40	400	SrF_2	$Fm-3m$	$a = 5.8001(1)$
16	14:29:57	400	SrF_2	$Fm-3m$	$a = 5.7992(1)$
17	22:33:45	300	"CaF_2" + "SrF_2"	$Fm-3m$	$a_1 = 5.483(1)$ $a_2 = 5.775(1)$
18	8:12:80	300	"CaF_2" + "SrF_2"	$Fm-3m$	$a_1 = 5.476(1)$ $a_2 = 5.784(1)$
19	17:50:33	300	"CaF_2" + "SrF_2"	$Fm-3m$	$a_1 = 5{,}479(1)$ $a_2 = 5.792(1)$
20	7:21:72	300	"CaF_2" + "SrF_2"	$Fm-3m$	$a_1 = 5.473(1)$ $a_2 = 5.789(1)$

* See Appendix A, Table A1.

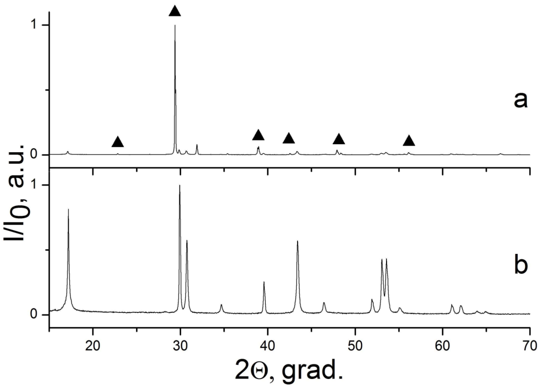

Figure 1. X-ray diffraction patterns of $NaYF_4$ sample 3 before (**a**) and after (**b**) washing with water. $NaNO_3$ phase lines are marked with triangle symbols.

Figure 2 data illustrate the influence of fluorinating agent stoichiometry on the phase composition of the reaction products. NaF shortage results in precipitation of the two-phase specimen (Figure 2a) containing $NaYF_4$ and yttrium fluoride. The SEM image of this sample (Figure 3a) indicates that this specimen contained particles of varying morphology: small (ca. 30 nm) spherical YF_3 particles and larger faceted single crystal $NaYF_4$ particles (ca. 100 nm). A further increase of the fluorinating agent stoichiometry in the starting reaction mixture caused a decrease in YF_3 content in the obtained products. Using $Y(NO_3)_3$:NaF:$NaNO_3$ = 7:52:41 starting material ratio has resulted in the precipitation of the single phase $NaYF_4$. It is worth mentioning that the $NaYF_4$ crystallization from the $NaNO_3$ melt is incongruent, so, in order to obtain a pure/uncontaminated product, one has to use an excess of fluorinating agent compared to the process (2) stoichiometry.

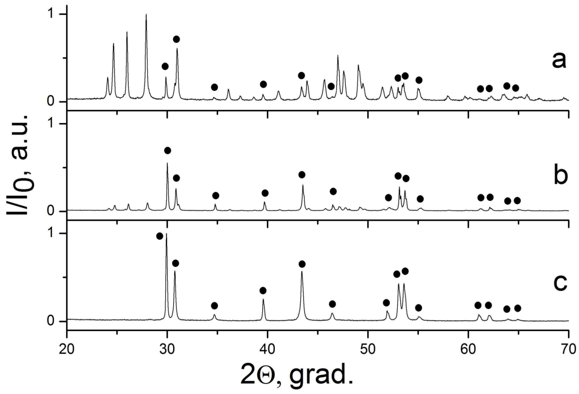

Figure 2. X-ray diffraction patterns of samples in the NaF–YF_3 system synthesized at 320 °C, ratios of $Y(NO_3)_3$:NaF:$NaNO_3$ starting materials: 11:30:59 (**a**) (sample 1); 9:39:52 (**b**) (sample 2); 7:52:41 (**c**) (sample 3). $NaYF_4$ phase lines are marked with solid circle symbols.

As our example with 3 and 4 samples of $Y(NO_3)_3$:NaF:$NaNO_3$ = 7:52:41 starting material ratio has demonstrated, raising the temperature of the specimen synthesis from 320 to 435 °C did not affect its X-ray diffraction pattern: in both cases, the synthesized products contained $NaYF_4$ phase only with nearly the same crystal lattice parameters (Table 1), but with different particle morphology (Figure 4). $NaYF_4$ particles, formed at 320 °C (Figure 4b,d), contained relatively large hexagonal-shaped micron-size particles. Such particles, made up by ca. 50 nm thick platelets, were hollow inside. In turn, a similar composition sample, formed at 320 °C (Figure 4b,d), also contained elongated micron-size particles with habitus, typical for the hexagonal system, but the temperature increase has led to the formation of dense, completely filled (bulk) particles.

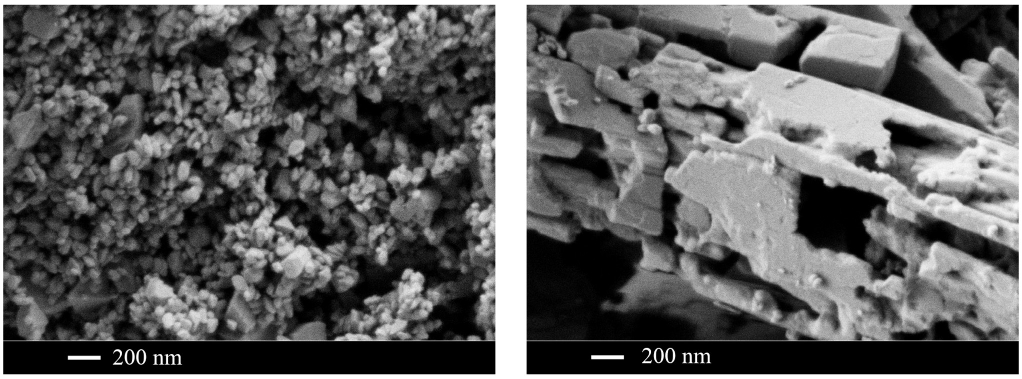

(**a**) (**b**)

Figure 3. *Cont.*

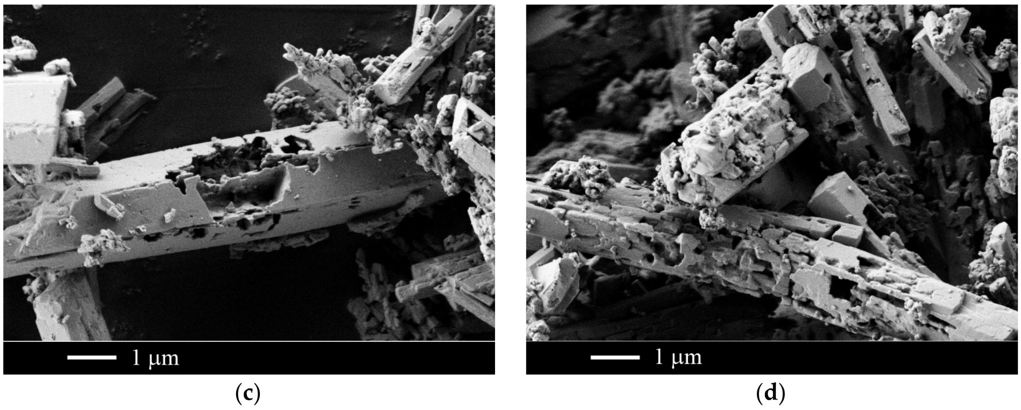

(**c**) (**d**)

Figure 3. Scanning electron microscopy (SEM) images of the specimens in the NaF–YF_3 system synthesized at 320 °C, ratios of $Y(NO_3)_3$:NaF:$NaNO_3$ starting materials: 11:30:59 (**a**) (sample 1); 9:39:52 (**b**) (sample 2); 7:52:41 (**c**) (sample 3); 9:39:52 (sample 2) (**d**).

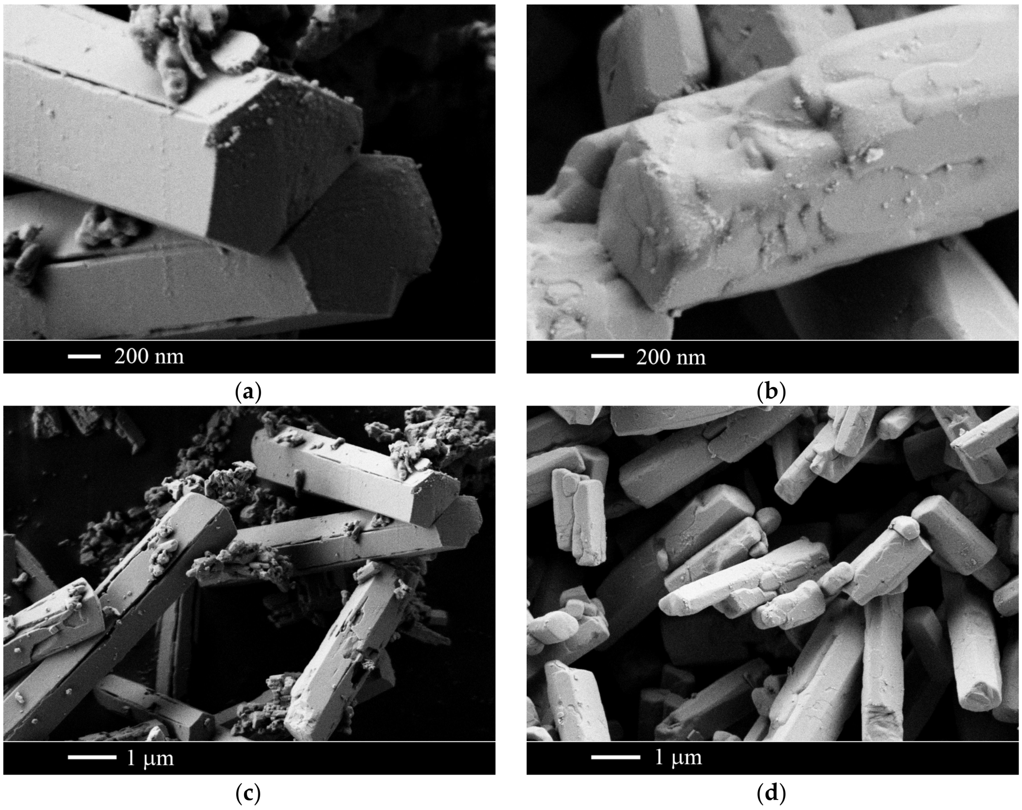

(**a**) (**b**)

(**c**) (**d**)

Figure 4. SEM images of $NaYF_4$ specimens (synthesized at ratios of $Y(NO_3)_3$:NaF:$NaNO_3$ starting materials equal to 7:52:41) synthesized at 320 °C (**a**,**c**) (sample 3); 435 °C (**b**,**d**) (sample 4).

2.2. The NaF–LaF_3 and NaF–CeF_3 Systems

Our attempts to prepare $NaLaF_4$ phase in the NaF–LaF_3 system were unsuccessful: for any ratios of the starting materials, only LaF_3 microcrystals were formed (Figure 5a).

$NaCeF_4$ phase easily precipitated in the NaF–CeF_3 system (Figure 5b). $NaCeF_4$ morphology (micron-sized hexagonal prisms) has been similar to $NaYF_4$ morphology (Figure 6).

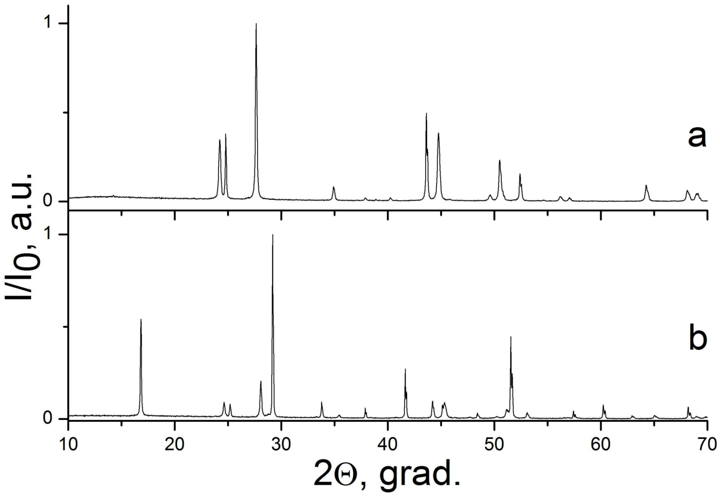

Figure 5. X-ray patterns of specimens in the NaF–LaF_3 and NaF–CeF_3 systems: Sample 6 (**a**), LaF_3 phase; and Sample 7 (**b**), $NaCeF_4$ + CeF_3 phases.

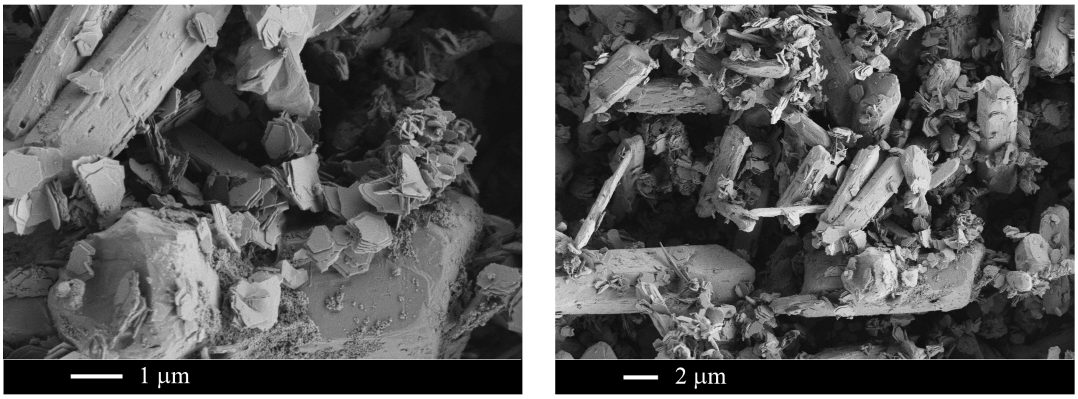

(**a**) (**b**)

Figure 6. SEM images of sample 7 in the NaF–CeF_3 system ($Ce(NO_3)_3$:NaF:$NaNO_3$ = 4:53:43 ratio of starting materials) synthesized at 400 °C.

2.3. The CaF_2–SrF_2 System

The results of our syntheses in the calcium and strontium fluoride systems are presented in Figures 7–11. The values of yield were 68–91% (see Appendix A, Table A2). Intrinsic fluorides form easily washable micron-sized particles with fluorite-type crystal structures (Figure 7) with lattice parameters coinciding with the literature data (CaF_2, a = 5.463 Å, PCPDFWIN # 35-0816; SrF_2, a = 5.800 Å, PCPDFWIN # 06-0262). However, the morphology of the aforementioned powder particles is different: strontium fluoride formed faceted particles, whereas calcium fluoride did not (Figure 8). The use of equimolar Ca:Sr = 1:1 starting composition produced a mixture of two different fluorite-type phases with crystal lattice parameters different from both unit cell parameters for intrinsic CaF_2 and SrF_2 (Figure 9). SEM data unequivocally indicate that fluoride particles, containing more strontium fluoride, had a much larger size than the particles, containing more calcium fluoride (Figures 10 and 11).

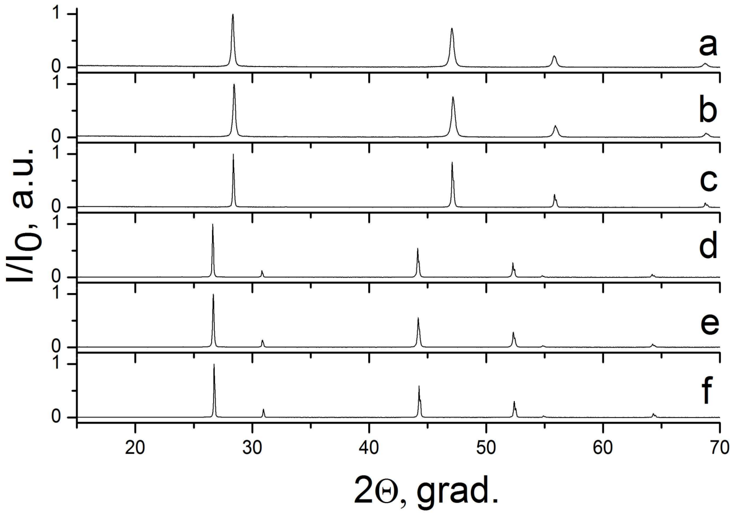

Figure 7. X-ray diffraction patterns of CaF_2: Samples 8 (**a**), 9 (**b**), 11 (**c**), and SrF_2: Samples 12 (**d**), 13 (**e**), 16 (**f**) specimens synthesized from $NaNO_3$ flux.

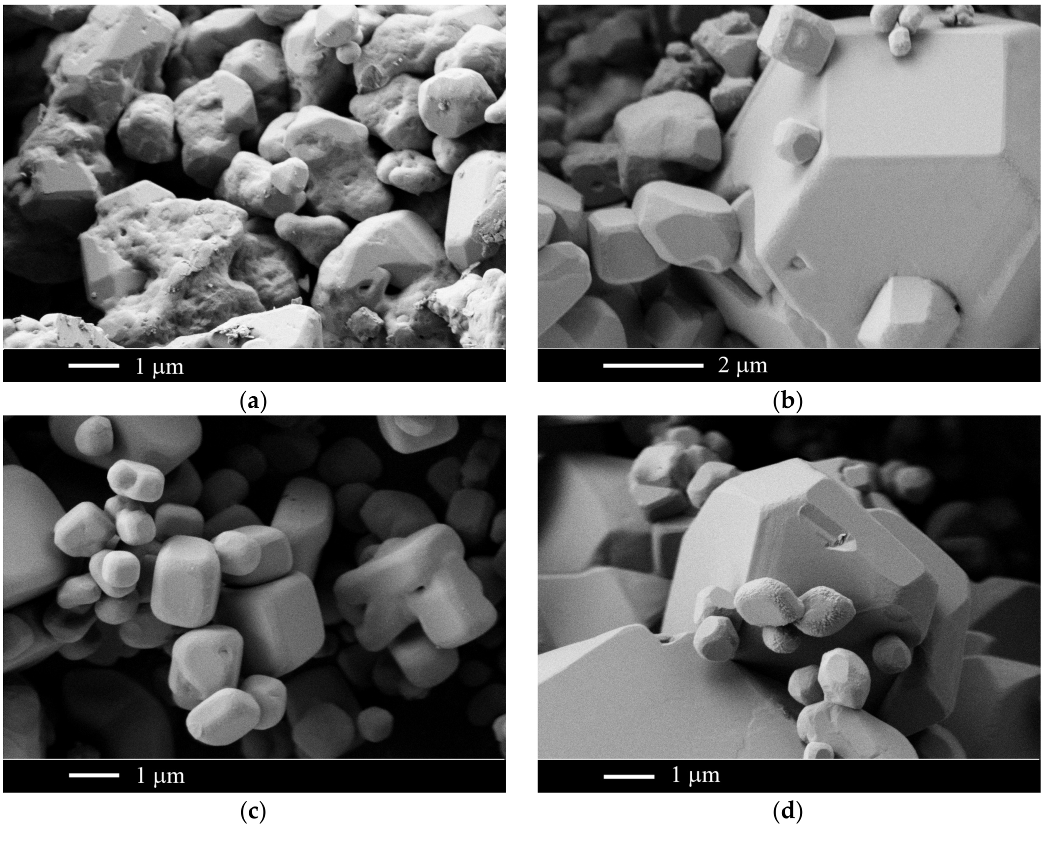

(**a**) (**b**)

(**c**) (**d**)

Figure 8. SEM images of CaF_2, sample 10 (**a**) and SrF_2 samples 15 (**b**), 14 (**c**), 15 (**d**).

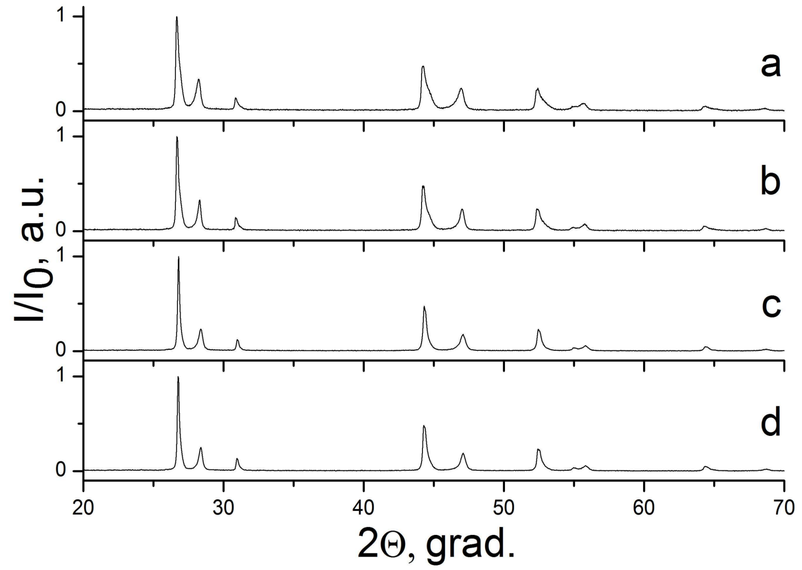

Figure 9. X-ray diffraction patterns of samples in the CaF_2–SrF_2 (1:1) system synthesized at 300 °C, ratios of $M(NO_3)_2$:NaF:$NaNO_3$ (M = Ca + Sr) starting materials: (**a**) 22:33:45 (sample 17); (**b**) 8:12:80 (sample 18); (**c**) 17:50:33 (sample 19); (**d**) 7:21:72 (sample 20).

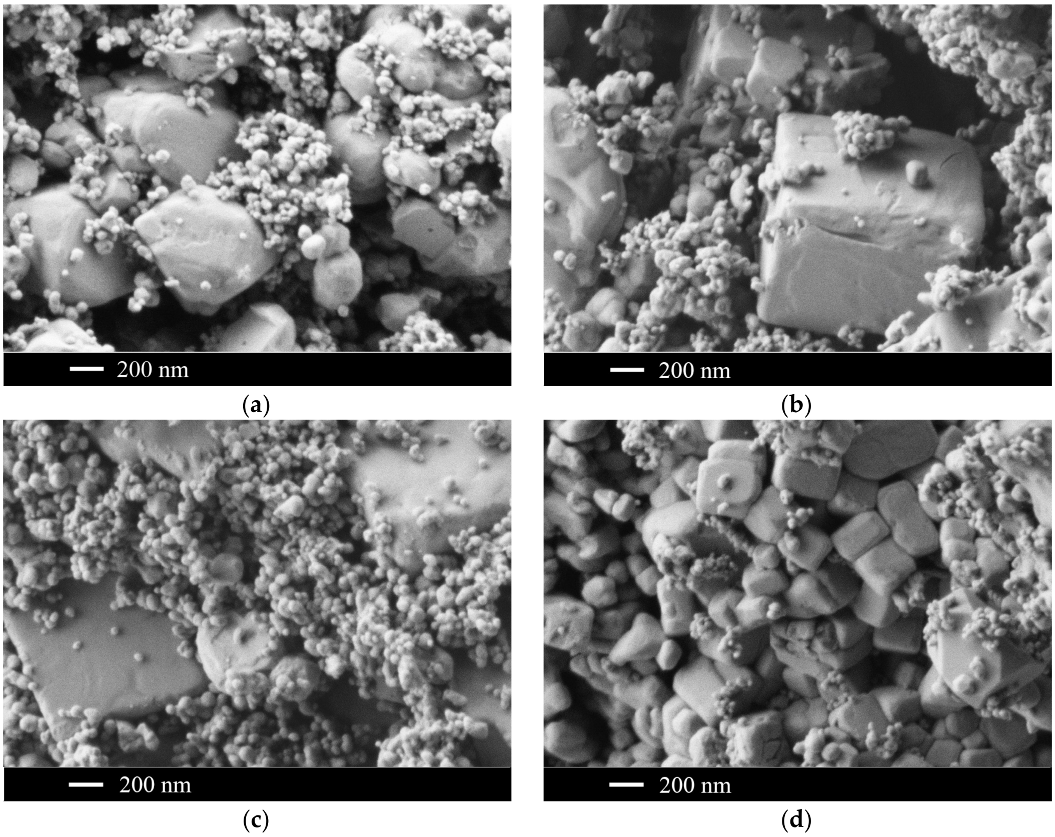

(**a**) (**b**)

(**c**) (**d**)

Figure 10. SEM images of CaF_2–SrF_2 (1:1) samples prepared at 300 °C and $M(NO_3)_2$:NaF:$NaNO_3$ (M = Ca + Sr) ratios of starting materials (mol %): 22:33:45 (sample 17) (**a**); 8:12:80 (sample 18) (**b**); 17:50:33 (sample 19) (**c**); and 7:21:72 (sample 20) (**d**).

3. Discussion

For the reader's convenience, the properties of molten sodium nitrate are summarized in Table 2.

Table 2. $NaNO_3$ properties [67].

Property	Symbol (Units)	Value
Melting point	t (°C)	305
Density	ρ (kg/m^3)	1903
Thermal conductivity	λ (W/m·K)	2.5×10^{-3}
Specific heat	Cp (J/kg·K)	2836
Thermal expansivity	β (K^{-1})	4.5×10^{-4}
Viscosity	m (kg/m·s)	2.2×10^{-3}

The solubility of NaF in $NaNO_3$ at 350 °C is about 5 mol %, and it increases up to 10 mol % at 450 °C [68]. Pure $NaNO_3$ decomposes at 557 °C, but its decomposition temperature lowers when NaF is added (the addition of 7 mol % NaF decreases the decomposition temperature to 502 °C) [69]. Nevertheless, the use of $NaNO_3$ melts provides a sufficiently broad temperature interval for the corresponding syntheses. Moreover, the addition of other nitrates and/or salts like KNO_3, NH_4NO_3, etc. can lower further the $NaNO_3$ melting temperature [70]: solid solution, formed in the $NaNO_3$–KNO_3 system, has its minimum point in the melting curves at 222 °C for 52 ± 3 mol % KNO_3 [71]. However, addition of the different cations in the molten reaction mixture unavoidably results in the contamination of the formed microcrystals and even in the parallel formation of supplementary parasitic phases [46].

Sodium nitrate is a well-known oxidizer, but it has not shown any oxidative properties in our experiments, including absence of Ce(III) to Ce(IV) oxidation (i.e., formation of Ce(IV) phases was not observed). Nevertheless, one has to monitor a possibility of such oxidation processes in the future.

The oxygen and nitrogen content in the synthesized samples are below the detection limit (1%) of the EDX method.

It is important to note that the simultaneous preparation of strontium and calcium fluorides has resulted in the formation of the mixture of slightly contaminated individual CaF_2 and SrF_2, respectively, whereas the use of the other synthetic techniques, such as melting [72], co-precipitation from aqueous solutions [28], or mechanochemical synthesis [73], resulted in continuous $Ca_{1-x}Sr_xF_2$ solid solution. However, in accordance with the third law of thermodynamics [24], all solid solutions must decompose under cooling, and the lack of such decomposition unequivocally indicates a non-equilibrium state of the prepared specimen. The highest critical decomposition temperature for $Ca_{1-x}Sr_xF_2$ solid solution, estimated for the CaF_2–SrF_2–MnF_2 triple system data, is about 1160 K [74]. The decomposition curve of the $Ca_{1-x}Sr_xF_2$ solid solution, calculated for the regular solution model, is presented in Figure 11. Taking into account crystal lattice parameters a = 5.463 Å for CaF_2 and a = 5.800 Å for SrF_2 and considering a linear correlation between crystal lattice parameters and composition of the $Ca_{1-x}Sr_xF_2$ solid solution (Vegard's Law), we carried out calculations for the concentrations of the CaF_2-based and SrF_2-based solid solutions (Table 3). We also used the data of Table 1 for the unit cell parameters of the phases formed in the CaF_2–SrF_2 system. The obtained 5 ± 2 mol % solid solution concentrations are in a good agreement with the estimated data for T = 573 K (Figure 11). At the present time, we plan to continue our investigations of the influence of the synthesis durations on the aforementioned crystal lattice parameters.

Table 3. Compositions of the specimens synthesized in the SrF_2–CaF_2 system.

Sample Number	Composition
17	$Ca_{0.94}Sr_{0.06}F_2 + Sr_{0.93}Ca_{0.07}F_2$
18	$Ca_{0.96}Sr_{0.04}F_2 + Sr_{0.95}Ca_{0.05}F_2$
19	$Ca_{0.95}Sr_{0.05}F_2 + Sr_{0.97}Ca_{0.03}F_2$
20	$Ca_{0.97}Sr_{0.03}F_2 + Sr_{0.97}Ca_{0.03}F_2$

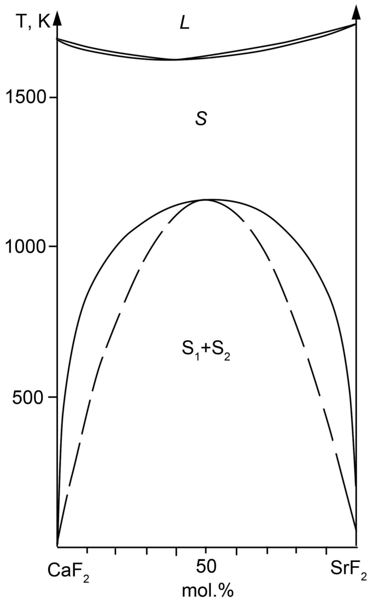

Figure 11. Phase diagram of the CaF_2–SrF_2 system [72]: melt (L), $Ca_{1-x}Sr_xF_2$ solid solution (S); spinodal is shown as a dashed line.

Therefore, in the aforementioned $Ca_{1-x}Sr_xF_2$ system, only the synthesis in the $NaNO_3$ melt produced equilibrium phases. This observation demonstrates quite unique perspectives for the preparation of the lower temperature equilibrium phases in the fluoride systems: making and studying such phases has been quite limited up to the present moment due to the above experimental obstacles [46,75,76]. Also, it is worth noting that the absence of $NaLaF_4$ in our synthesized specimens can be easily explained in view of the aforementioned observations, for $NaLaF_4$, easily obtainable by sintering or melting, is not stable at lower temperatures, while being stable at the higher temperatures [32,60,61].

It is worth mentioning the unusual morphology of the particles in synthesized $NaYF_4$ powders (Figures 3 and 4). It appears that flat nanoplates were formed first, and then they merged together forming hollow hexagonal prisms (Figures 3c and 4a,c), perhaps, by some attachment crystal growth process [40] with unknown/obscure mechanism. Bulk hexagonal prisms with habitus corresponding to the crystal lattice type have been formed at the higher temperature (Figure 4b,d).

Also it is worth mentioning the difference between morphologies of CaF_2 and SrF_2 microcrystals (Figure 8): SrF_2 microcrystals are faceted (see such simple-shaped polyhedral like cubes and rhombododecahedrons in the SEM images), but the faceting of CaF_2 was much fuzzier for unknown reasons. When both CaF_2-based and SrF_2-based solid solutions formed in the same precipitate, the particle size of the former is less than the particle size of the latter (Figures 10 and 11). Dissolution of CaF_2 in SrF_2 led to the lower quality faceting compared to the intrinsic SrF_2 (Figure 10).

Comparison of $NaNO_3$ and NH_4NO_3 melt properties provides the former with two advantages: (1) NH_4NO_3 is thermally unstable and easily undergoes solid state decomposition before reaching its melting point at 167 °C [77], producing toxic gases containing N_2O (one has to use hood exhaust equipment while working with NH_4NO_3 melts); and (2) as per Huang et al. [66], the use of NH_4NO_3 melts does not necessarily produce equilibrium conditions ("$BaCeF_5$" phase is absent in the BaF_2–CeF_3 phase diagram [2], so cubic solid solution had to undergo mandatory ordering that has yet to be observed in [66]).

The use of ionic liquids for nanofluoride preparation represents a separate synthesis venue [78–82]. Ionic liquids are salts, containing large organic cations (usually, the unsymmetric ones), melt below 100 °C, and possess good thermal stability, high fire hazard safety, low corrosive activity, along with the low viscosity and vapor pressure. Ionic liquids appear to be good solvents for various organic and inorganic chemical compounds. Typical examples of ionic liquids include 1-butyl-3-methylimidazolium hexafluorophosphate ($BmimPF_6$), tetrafluoroborate ($BmimBF_4$), and/or chloride (BmimCl) [83]. These ionic liquids have been used successfully for the LnF_3 and $NaLnF_4$ rare earth nanofluoride syntheses [78–82] as solvents (ionic transport media) and as fluorinating agents (water traces initiate ionic liquid pyrohydriolysis). Synthesized nanopowders can be easily separated from ionic liquids by rinsing with methanol. Usually, ionic liquid syntheses are carried out at the elevated temperatures under microwave or solvothermal process conditions.

Nevertheless, our $NaNO_3$ melt-based synthetic technique can be a good replacement or supplement to the aforementioned preparation methods in ionic liquids: $NaNO_3$ possesses the same advantages as the aforementioned ionic liquids (lower-temperature melting point, high fire hazard safety, low corrosive activity, low toxicity), but it also is less expensive and can be washed out with water instead of toxic and flammable methanol.

4. Materials and Methods

We used 99.99 wt % pure yttrium, lanthanum and cerium nitrate hexahydrates $Ln(NO_3)_3 \cdot 6H_2O$, calcium nitrate tetrahydrate $Ca(NO_3)_2 \cdot 4H_2O$ (all reagents were manufactured by LANHIT, Moscow, Russia), 99.9 wt % pure $Sr(NO_3)_2$, $NaNO_3$, and NaF (KhimMed, Moscow, Russia), and double distilled water as our starting materials without further purification.

We synthesized the fluoride specimens in $NaNO_3$ melts at 300–435 °C in ceramic crucibles with and without aluminum foil lining as well as in alundum crucibles. Separate experiments have indicated that ceramic crucibles were capable of withstanding melt corrosion, and metal lining did not provide any additional benefit to the quality and purity of the synthesized samples.

Starting materials were ground in the mortar with pestle until a homogeneous powder was formed. It was then quantitively transferred to the glazed porcelain crucible and placed in the oven for the synthesis at the elevated temperatures. Ratios of the starting materials were varied within the aforementioned ranges, including changes of the amounts of fluorinating agent excess and amount of the solvent used. All synthetic experiments were carried out at 300–435 °C (10 °C/min heating rate, 1 h exposure at maximum temperature) for all specimens unless specified otherwise. Annealed samples were cooled slowly over 10 hours. Molten products were removed from the crucibles, washed with doubly distilled water to remove remaining solvent and unreacted fluorinating agent, and dried under air at ~40 °C.

All synthesized samples were studied using a Bruker D8 Advanced (Cu $K\alpha$ radiation) diffractometer (Bruker AXS GmbH, Karlsruhe, Germany). Crystal lattice parameters were calculated with TOPAS 4.2 software package ($R_{wp} < 10$) (Bruker, Karlsruhe, Germany). The particle size and morphology (scanning electron microscopy, SEM) and the chemical composition (energy dispersive X-ray analysis, EDX) of the samples were analyzed on a NVision 40 high-resolution scanning electron microscope (Carl Zeiss NTS GmbH, Oberkochen, Germany) equipped with an XMAX (80 mm^2) detector (Oxford Instruments, Abingdon, UK), operating at an accelerating voltage of 1–20 kV. SEM images were obtained using an Everhart–Thornley detector (SE2) (Carl Zeiss NTS GmbH, Oberkochen, Germany).

5. Conclusions

Results of our experiments unequivocally indicate that $NaNO_3$ melt is a very promising medium for the preparation of inorganic fluoride materials over a broad temperature range (300–500 °C). The latter synthetic temperature can be further lowered by using nitrate mixture, e.g., $NaNO_3$–KNO_3. Syntheses in $NaNO_3$ melts allowed preparation of micron-sized powders containing faceted microcrystals with the lowered surface areas and decreased adsorption capabilities. The obtained luminescent materials did not require additional thermal treatment. Synthesized specimens contained equilibrium phases, and were not contaminated by oxygen and/or carbon. Suggested synthetic protocols are inexpensive, environmentally friendly and can be used as an alternative to ionic liquid synthesis methods.

Acknowledgments: This work has been carried out as a part of the planned GPI RAS research activity with the partial use of the equipment of the JRS PMR IGIC RAS. Authors express their sincere gratitude to Arthur I. Popov, Richard Simoneaux, and Elena Chernova for their most kind assistance in the preparation of the present manuscript.

Author Contributions: Pavel Fedorov and Mariya Mayakova conceived and designed the experiments; Mariya Mayakova, Alexander Alexandrov, Valery Voronov, and Alexander Baranchikov performed the experiments; Pavel Fedorov, Mariya Mayakova, and Vladimir Ivanov analyzed the data; Vladimir Ivanov and Sergey Kuznetsov contributed reagents/materials/analysis tools; Pavel Fedorov wrote the paper.

Conflicts of Interest: The authors declare no conflict of interest.

Appendix A

Table A1. Correspondence between the numbering of samples used in the paper and the current laboratory numbering of samples.

Paper Sample Number	Laboratory Sample Number
1	F1065
2	F1068
3	F1064a
4	F1064б
5	F1711
6	F1084
7	F1731
8	F1804
9	F1812
10	F1798
11	F1802
12	F1805
13	F1811
14	F1799
15	F1797
16	F1803
17	F1807
18	F1808
19	F1809
20	F1810

Table A2. The values of yield.

Paper Sample Number	Mass Theor., g	Mass Exp., g	Yield, %
8	5	4.35	87.0
9	5	4.59	91.8
10	5	3.90	78.0
12	5	4.32	86.4
13	5	3.77	75.4
14	5	2.99	59.8
15	5	4.18	83.6
17	5	4.34	86.8
18	5	4.55	91.0
19	5	3.98	79.6
20	5	3.84	76.8

References

1. Bergmann, H. Sc, Y, La and lanthanide: Fluoride, oxifluoride und zugehogige alkalidoppelverbindungen. In *Gmelin Handbuch der Anorganischen Chemie*; Springer: Berlin, Germany, 1976; ISBN 978-3-540-93321-2.
2. Sobolev, B.P. *The Rare Earth Trifluorides: The High Temperature Chemistry of the Rare Earth Trifluorides*; Institut d'Estudis Catalans: Barcelona, Spain, 2000; ISBN 84-7283-518-9.
3. Kuznetzov, S.V.; Osiko, V.V.; Tkatchenko, E.A.; Fedorov, P.P. Inorganic nanofluorides and related nanocomposites. *Russ. Chem. Rev.* **2006**, *7*, 1065–1082. [CrossRef]
4. Fedorov, P.P.; Luginina, A.A.; Kuznetsov, S.V.; Osiko, V.V. Nanofluorides. *J. Fluor. Chem.* **2011**, *132*, 1012–1039. [CrossRef]
5. Stosiek, C.; Scholz, G.; Schroeder, S.L.M.; Kemnitz, E. Structure and properties of noncrystalline aluminum oxide-hydroxide fluorides. *Chem. Mater.* **2010**, *22*, 2347–2356. [CrossRef]
6. Wilkening, M.; Duvel, A.; Preishuber-Pflugl, F.; Da Silva, K.; Breuer, S.; Sepelak, V.; Heitjans, P. Structure and ion dynamics of mechanosynthesized oxides and fluorides. *Z. Kristallog.* **2016**, *232*, 107–127. [CrossRef]
7. Warf, J.C.; Cline, W.D.; Tevebaugh, R.D. Pyrohydrolysis in the determination of fluoride and other halids. *Anal. Chem.* **1954**, *26*, 342–346. [CrossRef]
8. Banks, C.V.; Burke, K.E.; O'Laughlin, J.W. The determination of fluorine in rare earth fluorides by high temperature hydrolysis. *Anal. Chim. Acta* **1958**, *19*, 239–243. [CrossRef]
9. Sobolev, B.P.; Fedorov, P.P.; Steynberg, D.B.; Sinitsyn, B.V.; Shakhkalanian, G.S. On the problem of polymorphism and fusion of lanthanide trifluorides. I. Influence of oxygen on phase transition temperatures. *J. Solid State Chem.* **1976**, *17*, 191–199. [CrossRef]
10. Bamberger, C.E. Experimental Techniques in Molten Fluoride Chemistry. In *Advances in Molt Salt Chemistry*; Braunstein, J., Mamantov, G., Smith, G.P., Eds.; Plenum Press: New York, NY, USA, 1975; Volume 3, pp. 177–248.
11. Fedorov, P.P.; Osiko, V.V. Crystal growth of fluorides. In *Bulk Crystal Growth of Electronic, Optical and Optoelectronic Materials*; Capper, P., Ed.; John Wiley & Son, Ltd.: Chichester, UK, 2005; pp. 339–356.
12. Sobolev, B.P.; Fedorov, P.P. Phase diagramms of the CaF_2–(Y,Ln)F_3 systems. I. Experimental. *J. Less Common Met.* **1978**, *60*, 33–46. [CrossRef]
13. Fedorov, P.P. Anneal time determined by studying phase transitions in solid binary systems. *Russ. J. Inorg. Chem.* **1992**, *37*, 973–975.
14. Kuznetsov, S.V.; Fedorov, P.P. Morphological stability of solid–liquid interface during melt crystallization of solid solutions $M_{1-x}R_xF_{2+x}$. *Inorg. Mater.* **2008**, *44*, 1434–1458. [CrossRef]
15. Druon, F.; Ricaud, S.; Papadopoulos, D.N.; Pellegrina, A.; Camy, P.; Doualan, J.L.; Moncorge, R.; Courjaud, A.; Mattay, E.; Georges, P. On Yb:CaF_2 and Yb:SrF_2: Review of spectroscopic and thermal properties and their impact on femtosecond and high power laser performance. *Opt. Mater. Express.* **2011**, *1*, 489–502. [CrossRef]
16. Kaminskii, A.A.; Butashin, A.V.; Sul'yanov, S.N. Crystallization and some spectroscopic properties of $CsBi_2F_7$–Nd^{3+}. *Neorg. Mater.* **1996**, *32*, 110–112. (In Russian)
17. Matar, S.; Reau, J.-M.; Grannec, J.; Rabardel, L. On a low-temperature form of $KBiF_4$. *J. Solid State Chem.* **1983**, *50*, 1–6. [CrossRef]

18. Dombrovski, E.N.; Serov, T.V.; Abakumov, A.M.; Ardashnikova, E.I.; Dolgikh, V.A.; Van Tendeloo, G. The structural investigation of $Ba_4Bi_3F_{17}$. *J. Solid State Chem.* **2004**, *177*, 312–318. [CrossRef]
19. Ratnikova, I.D.; Korenev, Y.M.; Fedorov, P.P.; Sobolev, B.P. Phase diagrams of the systems BaF_2–RF_4 (R = Zr, Hf). *Zh. Neorgan. Khimii* **1997**, *42*, 302–307. (In Russian)
20. Popov, A.I.; Scharabarin, A.V.; Sukhoverkhov, V.F.; Tchumaevsky, N.A. Synthesis and properties of pentavalent antimony and bismuth fluorides. *Z. Anorg. Allgem. Chem.* **1989**, *576*, 242–254. [CrossRef]
21. Popov, A.I.; Valkovskii, M.D.; Kiselev, Y.M. Structure of $M^{II}(AuVF_6)_2$ of alkali-earth elements. *Zh. Neorgan. Khimii* **1990**, *35*, 1970–1977. (In Russian)
22. Buchinskaya, I.I.; Fedorov, P.P. Lead difluoride and related systems. *Rus. Chem. Rev.* **2004**, *73*, 371–400. [CrossRef]
23. Fedorov, P.P.; Zibrov, I.P.; Tarasova, E.V.; Polunina, S.M.; Sobolev, B.P.; Fedorov, P.I. Transition from peritectics to eutectics in PbF_2–RF_3 systems. *Zh. Neorgan. Khimii* **1988**, *33*, 3222–3225. (In Russian)
24. Fedorov, P.P. Third law of thermodynamics as applied to phase diagrams. *Rus. J. Inorg. Chem.* **2010**, *55*, 1722–1739. [CrossRef]
25. Heise, M.; Scholz, G.; Düvel, A.; Heitjans, P.; Kemnitz, E. Mechanochemical synthesis, structure and properties of lead containing alkaline earth metal fluoride solid solutions $M_xPb_{1-x}F_2$ (M = Ca, Sr, Ba). *Solid State Sci.* **2018**, *77*, 45–53. [CrossRef]
26. Ritter, B.; Krahl, T.; Rurack, K.; Kemnitz, E. Nanoscale CaF_2 doped with Eu^{3+} and Tb^{3+} through fluorolytic sol–gel Synthesis. *J. Mater. Chem. C* **2014**, *2*, 8607–8613. [CrossRef]
27. Glazunova, T.Y.; Boltalin, A.I.; Fedorov, P.P. Synthesis of calcium, strontium, and barium fluorides by thermal decomposition of trifluoroacetates. *Russ. J. Inorg. Chem.* **2006**, *51*, 983–987. [CrossRef]
28. Fedorov, P.P.; Kuznetsov, S.V.; Mayakova, M.N.; Voronov, V.V.; Ermakov, R.P.; Baranchikov, A.E.; Osiko, V.V. Coprecipitation from aqueous solutions to prepare binary fluorides. *Russ. J. Inorg. Chem.* **2011**, *56*, 1525–1531. [CrossRef]
29. Fedorov, P.P.; Mayakova, M.N.; Kuznetsov, S.V.; Voronov, V.V.; Osiko, V.V.; Ermakov, R.P.; Gontar', I.V.; Timofeev, A.A.; Iskhakova, L.D. Coprecipitation of barium–bismuth fluorides from aqueous solutions: Nanochemical effects. *Nanotechnol. Russ.* **2011**, *6*, 203–210. [CrossRef]
30. Fedorov, P.P.; Mayakova, M.N.; Kuznetsov, S.V.; Voronov, V.V.; Ermakov, R.P.; Samarina, K.S.; Popov, A.I.; Osiko, V.V. Co-precipitation of yttrium and barium fluorides from aqueous solutions. *Mater. Res. Bull.* **2012**, *47*, 1794–1799. [CrossRef]
31. Mayakova, M.N.; Luginina, A.A.; Kuznetsov, S.V.; Voronov, V.V.; Ermakov, R.P.; Baranchikov, A.E.; Ivanov, V.K.; Karban, O.V.; Fedorov, P.P. Synthesis of SrF_2–YF_3 nanopowders by co-precipitation from aqueous solutions. *Mendeleev Commun.* **2014**, *24*, 360–362. [CrossRef]
32. Kuznetsov, S.V.; Ovsyannikova, A.A.; Tupitsyna, E.A.; Yasyrkina, D.S.; Voronov, V.V.; Fedorov, P.P.; Batyrev, N.I.; Iskhakova, L.D.; Osiko, V.V. Phase formation in LaF_3-$NaGdF_4$, $NaGdF_4$-$NaLuF_4$, $NaYF_4$-$NaLuF_4$ systems: Synthesis of powders by co-precipitation from aqueous solutions. *J. Fluor. Chem.* **2014**, *161*, 95–101. [CrossRef]
33. Mayakova, M.N.; Voronov, V.V.; Iskhakova, L.D.; Kuznetsov, S.V.; Fedorov, P.P. Low-temperature phase formation in the BaF_2-CeF_3 system. *J. Fluor. Chem.* **2016**, *187*, 33–39. [CrossRef]
34. Fedorov, P.P.; Kuznetsov, S.V.; Osiko, V.V. Elaboration of nanofluorides and ceramics for optical and laser applications. In *Photonic and Electronic Properties of Fluoride Materials*; Tressaud, A., Poeppelmeier, K., Eds.; Elsevier: Amsterdam, The Netherlands, 2016; pp. 7–31. ISBN 9780128016398.
35. Fedorov, P.P.; Luginina, A.A.; Ermakova, Y.A.; Kuznetsov, S.V.; Voronov, V.V.; Uvarov, O.V.; Pynenkov, A.A.; Nischev, K.N. Preparation of nanodispersed fluorite-type $Sr_{1-x}R_xF_{2+x}$ (R = Er, Yb, Ho) phases from citrate solutions. *J. Fluor. Chem.* **2017**, *194*, 8–15. [CrossRef]
36. Fedorov, P.P.; Mayakova, M.N.; Kuznetsov, S.V.; Voronov, V.V.; Ermakova, Y.A.; Baranchikov, A.E. Synthesis of CaF_2–YF_3 nanopowders by co-precipitation from aqueos solutions. *Nanosystems* **2017**, *8*, 462–470. [CrossRef]
37. Luginina, A.A.; Baranchikov, A.E.; Popov, A.I.; Fedorov, P.P. Preparation of barium monohydrofluoride $BaF_2 \cdot HF$ from nitrate aqueous solutions. *Mater. Res. Bull.* **2014**, *49*, 199–205. [CrossRef]
38. Rozhnova, Y.A.; Luginina, A.A.; Voronov, V.V.; Ermakov, R.P.; Kuznetsov, S.V.; Ryabova, A.V.; Pominova, D.V.; Arbenina, V.V.; Osiko, V.V.; Fedorov, P.P. White light luminophores based on $Yb^{3+}/Er^{3+}/Tm^{3+}$-Coactivated strontium Fluoride Powders. *Mater. Chem. Phys.* **2014**, *148*, 201–207. [CrossRef]

39. Rozhnova, Y.A.; Kuznetsov, S.V.; Luginina, A.A.; Voronov, V.V.; Ryabova, A.V.; Pominova, D.V.; Ermakov, R.P.; Usachev, V.A.; Kononenko, N.E.; Baranchikov, A.E.; et al. New $Sr_{1-x-y}R_x(NH_4)_yF_{2+x-y}$ (R = Yb, Er) solid solution as precursor for high efficiency up-conversion luminophor and optical ceramics on the base of strontium fluoride. *Mater. Chem. Phys.* **2016**, *172*, 150–157. [CrossRef]
40. Ivanov, V.K.; Fedorov, P.P.; Baranchikov, A.Y.; Osiko, V.V. Oriented aggregation of particles: 100 years of investigations of non-classical crystal growth. *Russ. Chem. Rev.* **2014**, *83*, 1204–1222. [CrossRef]
41. Fedorov, P.P.; Kuznetsov, S.V.; Voronov, V.V.; Yarotskaya, I.V.; Arbenina, V.V. Soft chemical synthesis of $NaYF_4$ nanopowders. *Russ. J. Inorg. Chem.* **2008**, *53*, 1681–1685. [CrossRef]
42. Lucier, B.E.G.; Johnston, K.E.; Arnold, D.C.; Lemyre, J.-L.; Beaupre, A.; Blanchette, M.; Ritcey, A.M.; Schurko, R.W. Comprehensive solid-state characterization of rare earth fluoride nanoparticles. *J. Phys. Chem. C* **2014**, *118*, 1213–1228. [CrossRef]
43. Khaidukov, N.M.; Fedorov, P.P.; Dem'yanrts, L.D.; Zibrov, I.P.; Malyusov, V.A. K_2LnF_5 compounds. *Russ. J. Inorg. Chem.* **1990**, *35*, 383–384. (In Russian)
44. Khaidukov, N.M.; Fedorov, P.P.; Abramov, N.A. Thermal and crystallographic charasteristics of $KLnF_4$ synthesized under hydrothermal conditions. *Inorg. Mater.* **1991**, *27*, 2243–2246. (In Russian)
45. Khaidukov, N.M.; Filatova, T.G.; Ikrami, M.B.; Fedorov, P.P. Morphotropy in lanthanide fluoride series. *Inorg. Mater.* **1993**, *29*, 1152–1156. (In Russian)
46. Fedorov, P.P. Systems of alcali and rare-earth metal fluorides. *Russ. J. Inorg. Chem.* **1999**, *44*, 1703–1727.
47. Cao, J.; Yuan, L.; Hu, S.; Tang, J.; Zhou, X.; Yang, J. Tuning the phase, morphology and size of monodisperse ScF_3 and $NaScF_4$ crystals through lanthanide doping. *CrystEngComm* **2016**. [CrossRef]
48. Kostiv, U.; Rajsiglov, L.; Luptáková, D.; Pluháček, T.; Vannucci, L.; Havliček, V.; Engstová, H.; Jirák, D.; Šlouf, M.; Makovicky, P.; et al. Biodistribution of upconversion/magnetic silicacoated $NaGdF_4$:Yb^{3+}/Er^{3+} nanoparticles in mouse models. *RSC Adv.* **2017**, *7*, 45997–46006. [CrossRef]
49. Hyppänen, I.; Perälä, N.; Arppe, R.; Schäferling, M.; Soukka, T. Environmental and excitation power effects on the ratiometric upconversion luminescence based temperature sensing using nanocrystalline $NaYF_4$:Yb^{3+},Er^{3+}. *ChemPhysChem* **2017**, *18*, 692–701. [CrossRef]
50. Timofeeva, V.A. *Physical-Chemical and Metodical Bases of Melt-Solution Design of New Technical Crystals*; VINITI: Moscow, Russia, 1990; p. 498. (in Russian)
51. Pavlova, L.N.; Fedorov, P.P.; Ol'khovaya, L.A.; Ikrami, D.D.; Sobolev, B.P. Ordering of heterovalent solid solution with the fluorite structure in the NaF–BaF_2–GdF_3 system. *Crystallogr. Rep.* **1993**, *38*, 221–224.
52. Garton, G.; Wanklyn, B.M. Growth of complex fluoride single crystals by the flux method. *J. Cryst. Growth* **1967**, *1*, 49–51. [CrossRef]
53. Hoppe, R. Novel routs to the synthesis of metal fluorides. *J. Fluor. Chem.* **1985**, *29*, 38. [CrossRef]
54. Wang, W.; Liu, X.; Zhang, J.; Ji, Y.; Jiang, N.; Ma, B.; Wang, X.; Liu, L. A facile way to synthesis $KMgF_3$ and its luminescent property with Eu doping. *Inorg. Chem. Commun.* **2013**, *33*, 165–169. [CrossRef]
55. Courbion, G.; Randrianohavy, J.V.; Rousseau, J.J. ESR Study of Cr^{3+} and Fe^{3+} Ions in $KGaF_4$ Single Crystals. *J. Solid State Chem.* **1989**, *81*, 285–292. [CrossRef]
56. Fedorov, P.P.; Mayakova, M.N.; Kuznetsov, S.V.; Maslov, V.A.; Sorokin, N.I.; Baranchikov, A.E.; Ivanov, V.K.; Pynenkov, A.A.; Uslamina, M.A.; Nishchev, K.N. Phase diagram of the NaF–CaF_2 system and the electrical conductivity of a CaF_2-based solid solution. *Russ. J. Inorg. Chem.* **2016**, *61*, 1472–1478. [CrossRef]
57. Fedorov, P.P.; Mayakova, M.N.; Maslov, V.A.; Baranchikov, A.E.; Ivanov, V.K.; Pynenkov, A.A.; Uslamina, M.A.; Nishchev, K.N. The solubility of sodium and potassium fluorides in the strontium fluoride. *Nanosystems* **2017**, *8*, 830–834. [CrossRef]
58. Fedorov, P.P.; Luginina, A.A.; Popov, A.I. Transparent oxyfluoride glass ceramics. *J. Fluor. Chem.* **2015**, *172*, 22–50. [CrossRef]
59. Morris, E.; Groy, T.; Leinenweber, K. Crystal structure and bonding in the high-temperature form of fluorite (CaF_2). *J. Phys. Chem. Solids* **2001**, *62*, 1117–1122. [CrossRef]
60. Batsanova, L.R. Rare-earth fluorides. *Russ. Chem. Rev.* **1971**, *40*, 465–484. [CrossRef]
61. Batsanova, L.R.; Kupriyanova, A.K.; Doroshenko, V.I. Study of the interaction of the rare-earth nitrates with sodium fluorides in molten $NaNO_3$. *Inorg. Mater.* **1971**, *7*, 1876–1877. (In Russian)
62. Ding, M.; Lu, C.; Cao, L.; Huang, W.; Ni, Y.; Xu, Z. Molten salt synthesis of tetragonal $LiYF_4$:Yb^{3+}/Ln^{3+} (Ln = Er, Tm, Ho) microcrystals with multicolor upconversion luminescence. *CrystEngComm* **2013**, *15*, 6015–6021. [CrossRef]

63. Huang, X.Y.; Hu, G.H.; Xu, Q.J.; Li, X.X.; Yu, Q.M. Molten-salt synthesis and upconversion of hexagonal $NaYF_4$:Er^{3+}:Yb^{3+} micro-/nano-crystals. *J. Alloys Compd.* **2014**, *616*, 652–661. [CrossRef]
64. Huang, X.Y. Synthesis in NH_4NO_3 flux and abnormal upconversion of $LiYF_4$:Er^{3+} /Yb^{3+} microcrystals. *Opt. Mater. Exp.* **2014**, *4*, 2381–2391. [CrossRef]
65. Huang, X.; Jiang, L.; Xu, Q.; Li, X.; He, A. Low-temperature molten-salt synthesis and upconversion of novel hexagonal $NaBiF_4$:Er^{3+}+/Yb^{3+} micro-/nanocrystals. *RSC Adv.* **2017**, *7*, 41190–41203. [CrossRef]
66. Huang, X.; Jiang, L.; Li, X.; He, A. Manipulating upconversion emission of cubic $BaGdF_5$:Ce^{3+}/Er^{3+}/Yb^{3+} nanocrystals through controlling Ce^{3+} doping. *J. Alloys Compd.* **2017**, *721*, 374–382. [CrossRef]
67. Sadovskiy, A.; Sukhanova, E.; Belov, S.; Kostikov, V.; Zykova, M.; Artyushenko, M.; Zharikov, E.; Avetissov, I. Axial vibration control of melt structure of sodium nitrate in crystal growth process. *J. Cryst. Growth* **2015**, *417*, 16–24. [CrossRef]
68. Nyankovskaya, R.N.; Bergman, A.G. Singular irreversible-resiprocal system from nitrates and fluorides of sodium and potassium. *Izv. Sektora Phys. Khim Anal.* **1952**, *21*, 250–258. (In Russian)
69. Kruglov, A.I.; Kochergin, V.P. Onset of thermal decomposition of mixtures of sodium and potassium nitrates with its halogenides. *Izv. VUZov Khimiya Khim Tekhnol.* **1971**, *14*, 1429–1430. (In Russian)
70. Voskresenskaya, N.K.; Evseeva, N.N.; Berul, S.I.; Vereschetina, I.P. *Handbook on the Melting of Salt Systems*; Izd. Akad. Nauk: Moscow, Russia, 1961; p. 848. (In Russian)
71. Greis, O.; Bahamdam, K.M.; Uwais, B.M. The phase diagram of the system $NaNO_3$–KNO_3 studied by differential scanning calorimetry. *Thermochim. Acta* **1985**, *86*, 343–350. [CrossRef]
72. Fedorov, P.P.; Ushakov, S.N.; Uslamina, M.A.; Chernova, E.V.; Kuznetsov, S.V.; Voronov, V.V.; Düvel, A.; Heitjans, P.; Pynenkov, A.A.; Nishchev, K.N.; et al. Morphological stability of the solid-liquid interface during melt crystallization of $Ca_{1-x}Sr_xF_2$ solid solution. *Crystallogr. Rep.* **2018**, *63*, 512–516.
73. Heise, M.; Scholz, G.; Düvel, A.; Heitjans, P.; Kemnitz, E. Mechanochemical synthesis, structure, and properties of solid solutions of alkaline earth metal fluorides: $M^a{}_{1-x}M^b{}_xF_2$ (M: Ca, Sr, Ba). *Solid State Sci.* **2016**, *60*, 65–74. [CrossRef]
74. Ol'khovaya, L.A.; Karpenko, G.A.; Ikrami, D.D.; Fedorov, P.P. The CaF_2–SrF_2–MnF_2 ternary system. *Russ. J. Inorg. Chem.* **1991**, *36*, 1639–1642.
75. Fedorov, P.P.; Izotova, O.E.; Alexandrov, V.B.; Sobolev, B.P. New phases with fluorite-derived structure in CaF_2–(Y, Ln)F_3 systems. *J. Solid State Chem.* **1974**, *9*, 368–374. [CrossRef]
76. Fedorov, P.P.; Sobolev, B.P.; Belov, S.F. Fusibility diagram of the system NaF–YF_3, and the cross-section $Na_{0.4}Y_{0.6}F_{2.2}$–YOF. *Inorg. Mater.* **1979**, *15*, 640–643.
77. Galwey, A.K.; Brown, M.E. *Thermal Decomposition of Ionic Solids*; Elsevier Science: Amsterdam, The Netherlands, 1999; ISBN 0-444-82437-5.
78. Zhang, C.; Chen, J. Facile EG/ionic liquid interfacial synthesis of uniform RE^{3+} doped $NaYF_4$ nanocubes. *Chem. Commun.* **2010**, *46*, 592–594. [CrossRef] [PubMed]
79. Guo, H.; Zhang, T.; Qiao, Y.M.; Zhao, L.H.; Li, Z.Q. Ionic liquid-based approach to monodisperse luminescent LaF_3:Ce, Tb nanodiskettes: Synthesis, structural and photoluminescent properties. *J. Nanosci. Nanotechnol.* **2010**, *10*, 1913–1919. [CrossRef] [PubMed]
80. Song, Y.; Deng, Y.; Chen, J.; Zou, H. Ionic liquid-assisted hydrothermal synthesis of rare earth luminescence materials. In *Application of Ionic Liquids on Rare Earth Green Separation and Utilization, Green Chemistry and Sustainable Technology*; Chen, J., Ed.; Springer: Heidelberg/Berlin, Germany, 2016; pp. 207–257.
81. Liu, S.; Hui, Y.; Zhu, L.; Fan, X.; Zou, B.; Cao, X. Synthesis and luminescence properties of CeF_3:Tb^{3+} nanodisks via ultrasound assisted ionic liquid method. *J. Rare Earths* **2014**, *32*, 508–513. [CrossRef]
82. Bartůněk, V.; Pinc, J.; Ulbrich, P.; Rak, J.; Pelánková, B.; Král, V.; Kuchař, M.; Ježek, P.; Engstová, H.; Smolková, K. Tunable rapid microwave synthesis of up-converting hexagonal $NaY_xGd_yYb_zEr_{(1-x-y-z)}F_4$ nanocrystals in large quantity. *J. Fluor. Chem.* **2015**, *178*, 56–60. [CrossRef]
83. Mun, J.; Sim, H. (Eds.) *Handbook of Ionic Liquids: Properties, Applications and Hazards*; NOVA Science Publishers, Inc.: New York, NY, USA, 2012; ISBN 978-1-62100-349-6.

© 2018 by the authors. Licensee MDPI, Basel, Switzerland. This article is an open access article distributed under the terms and conditions of the Creative Commons Attribution (CC BY) license (http://creativecommons.org/licenses/by/4.0/).